Prepared for submission to JHEP MPP-2013-226

NLO QCD corrections to diphoton plus jet production through graviton exchange

Nicolas Greiner[a], **Gudrun Heinrich**[a], **Joscha Reichel**[a], **Johann Felix von Soden-Fraunhofen**[a]

[a] *Max Planck Institut für Physik, Föhringer Ring 6, 80805 München, Germany*

E-mail: greiner@mpp.mpg.de, gudrun@mpp.mpg.de, joscha@mpp.mpg.de, jfsoden@mpp.mpg.de

Abstract: We present the NLO QCD corrections to the production of a photon pair in association with one jet, where the photons are stemming from graviton decay, within models of large extra dimensions. Our results for the loop amplitudes are produced with the program GoSam for automated one-loop calculations. We show distributions for several observables for 4, 5 and 6 extra dimensions and demonstrate that the differential K-factors are far from being uniform.

Keywords: Hadron colliders, NLO calculations, Beyond the Standard Model, Extra dimensions

arXiv:1308.2194v1 [hep-ph] 9 Aug 2013

Contents

1 Introduction **1**

2 Calculational framework **3**
- 2.1 The graviton propagator in large extra dimensions 3
- 2.2 Details of the implementation 4

3 Phenomenological results **7**
- 3.1 Setup, input parameters and cuts 7
- 3.2 Results 8

4 Conclusions **14**

1 Introduction

The discovery of a new boson at the LHC [1, 2] constitutes a big step towards unveiling the mechanism of electroweak symmetry breaking. However, it is still a major task to make sure that this new particle is indeed the Standard Model Higgs boson. Therefore it is important to scrutinize its coupling strengths, decay modes, and parity/spin quantum numbers. For the latter, the currently analyzed data strongly point to a CP even spin zero particle [3–8]. While a graviton-like spin-2 resonance with mass around 125 GeV is excluded at the 99% confidence level [3, 9, 10], models involving gravitons with masses in the TeV range are still a viable extension of the Standard Model. Even though graviton masses up to about 4 TeV are excluded at 95% CL for $\delta \leq 4$ extra dimensions with simple model assumptions [11–14], this can definitely not be interpreted in the sense that the existence of gravitons in the context of models involving extra dimensions is ruled out.

In models with flat extra dimensions, in particular the ones proposed by ADD [15] with $D = 4 + \delta$ dimensions, only the gravitons propagate in the full D-dimensional spacetime, while the Standard Model fields are confined to four dimensions. If the δ-dimensional space is assumed to be compactified on a torus with common radius R, the 4-dimensional Planck scale $M_{\rm Pl} \sim 10^{19}$ GeV is an effective scale, related to the fundamental scale M_D of quantum gravity by [15]

$$M_{\rm Pl}^2 = 8\pi R^\delta M_D^{\delta+2}. \tag{1.1}$$

For large values of the compactification radius R it is therefore possible to have a fundamental scale $M_D \sim 1$ TeV. Alternatively, the string scale M_S is often used instead of M_D in the literature [16]. The two scales are related by [17]

$$M_S^{\delta+2} = (4\pi)^{\frac{\delta+2}{2}} \Gamma(\delta/2) M_D^{\delta+2} \,. \tag{1.2}$$

As the extra-dimensions are assumed to be compact, the discrete Fourier decomposition of the graviton states leads to a tower of Kaluza-Klein (KK) modes in four dimensions with spacings of the order of the inverse size of the extra dimensions. Within the ADD model [15] of large extra dimensions, the number of expected KK graviton states is very large, thus compensating the smallness of the individual graviton couplings to Standard Model matter. The excited graviton states preferably decay into gauge bosons, rather than fermions, because the spin-2 nature implies that fermions cannot be produced in an s-wave [16]. Therefore, and due to the clean experimental signature, the decay of graviton modes into two photons is of particular phenomenological interest.

At the LHC, searches for extra dimensions in diphoton events have been carried out [11–14], and have lead to lower limits on the scale M_S between 2.5 TeV and 3.92 TeV, depending on the number of extra dimensions and assumptions on model parameters. On the theory side, NLO corrections for the process $pp \to G \to \gamma\gamma$ have been calculated in [18, 19], supplemented by a parton shower in [20, 21], based on extensions to the `MadGraph/MadEvent` framework for spin-2 particles [22]. Ref. [21] also discusses the case where the coupling strength of the graviton to matter fields and gauge fields is non-universal, while Ref. [23] considers graviton decays into massive vector boson pairs rather than photons. The experimental analyses searching for extra dimensions in diphoton events have been carried out using a constant K-factor based on the results of [18, 19] to account for NLO corrections.

Diphotons at the LHC will often be accompanied by one or more high-p_T jets. Compared to the diphoton inclusive case, observables involving an extra jet offer better control on backgrounds and more information on the interaction dynamics. Therefore precise predictions for the production of diphotons through the exchange of a spin-2 particle in association with a hard jet can help to derive improved limits on models involving graviton exchange. This is particularly important since the K-factors turn out not to be uniform over the range of the diphoton invariant mass distribution, which in general is used to derive exclusion limits. Further, observables which serve to determine spin/CP properties of the object(s) leading to photons in the final state can be altered at NLO as new helicity configuration channels may open up, thus invalidating leading order studies. The NLO QCD corrections to the production of stable gravitons in association with a jet have been calculated in [24]. The phenomenology of spin-2 resonances produced by vector boson fusion is studied at NLO QCD in [25, 26], in an effective Lagrangian approach. NLO corrections to the Standard Model process $pp \to \gamma\gamma$+jet+X have been calculated in [27, 28], where the K-factors turned out to be rather large.

This article is organized as follows. In Section 2, we discuss details of the calculation, in particular the treatment of the graviton propagator and the implementation of a general framework for spin-2 particles into the one-loop program package GoSam. In Section 3 we present numerical results, followed by our conclusions in Section 4.

2 Calculational framework

2.1 The graviton propagator in large extra dimensions

For the Feynman rules, we follow the conventions of [16]. The Lagrangian for the interactions of the graviton Kaluza-Klein (KK) modes with the Standard Model matter proceeds via the energy-momentum tensor $T^{\mu\nu}$

$$\mathcal{L}_{Int} = -\frac{\kappa}{2}\sum_{\vec{n}} G^{(\vec{n})}_{\mu\nu} T^{\mu\nu} \,, \tag{2.1}$$

where κ is related to the reduced Planck mass in 4 dimensions by $\kappa = \sqrt{16\pi}/M_{\rm Pl}$, and the graviton modes follow the equation

$$\left(\Box + \frac{4\pi^2\vec{n}^2}{R^2}\right) G^{(\vec{n})}_{\mu\nu} = -\frac{\kappa}{2} T_{\mu\nu} \,. \tag{2.2}$$

The KK mode propagator can be split into two parts

$$i\Delta_{\mu\nu,\rho\sigma}(k, m_{\vec{n}}) = \underbrace{\frac{i}{k^2 - m^2_{\vec{n}} + i\epsilon}}_{D(k^2, m_{\vec{n}})} B_{\mu\nu,\rho\sigma}(k, m_{\vec{n}}) \,, \tag{2.3}$$

where $B_{\mu\nu,\rho\sigma}$ carries the Lorentz structure

$$\begin{aligned} B_{\mu\nu,\rho\sigma}(k, m) = &\left(\eta_{\mu\rho} - \frac{k_\mu k_\rho}{m^2}\right)\left(\eta_{\nu\sigma} - \frac{k_\nu k_\sigma}{m^2}\right) + \left(\eta_{\mu\sigma} - \frac{k_\mu k_\sigma}{m^2}\right)\left(\eta_{\nu\rho} - \frac{k_\nu k_\rho}{m^2}\right) \\ &- \frac{2}{3}\left(\eta_{\mu\nu} - \frac{k_\mu k_\nu}{m^2}\right)\left(\eta_{\rho\sigma} - \frac{k_\rho k_\sigma}{m^2}\right) \,. \end{aligned} \tag{2.4}$$

If all particles attached to the propagator are on-shell, the mass dependent terms in $B_{\mu\nu,\rho\sigma}(k, m)$ drop out. For the calculation presented here, the on-shell condition is not always fulfilled, but we checked that the impact of the mass dependent terms is numerically negligible[1] and therefore did not include them in our calculation. In this case the summation over the graviton states in $D(s, m_{\vec{n}})$, leading to

$$D(s) = \sum_{\vec{n}} \frac{i}{s - m^2_{\vec{n}} + i\epsilon} \,, \tag{2.5}$$

can be performed independently from the $B_{\mu\nu,\rho\sigma}$ part carrying the Lorentz structure. Further, we use the assumption that the widths of the KK modes are negligible, as the dominant effects come from the almost on-shell production of KK modes. The discrete spectrum of the KK modes can be approximated by an integral over a mass density, as the KK modes are very contiguous [16, 29]. The density as a function of the mass $m_{\vec{n}}$ is given by

$$\rho(m_{\vec{n}}) = \frac{R^\delta m^{\delta-2}_{\vec{n}}}{(4\pi)^{\delta/2}\Gamma(\delta/2)} \,, \tag{2.6}$$

[1] The same has been found in [17].

leading to [16]

$$D(s) \to \int_0^{M_S} d\, m_{\vec{n}}^2\, \rho(m_{\vec{n}})\, \frac{i}{s - m_{\vec{n}}^2 + i\epsilon} = \begin{cases} \frac{s^{\delta/2-1}}{2M_s^{\delta+2}G_N} \left(\pi + 2i\, I(\frac{M_S}{\sqrt{s}})\right) & \text{for } s > 0 \\ \frac{(-s)^{\delta/2-1}}{2M_s^{\delta+2}G_N}(-2i)\, I_E(\frac{M_S}{\sqrt{-s}}) & \text{for } s < 0 \end{cases} \tag{2.7}$$

with

$$I(x) = \begin{cases} -\sum_{k=1}^{\delta/2-1} \frac{1}{2k} x^{2k} - \frac{1}{2}\log(x^2-1) & \text{if } \delta \text{ even} \\ -\sum_{k=1}^{(\delta-1)/2} \frac{1}{2k-1} x^{2k-1} + \frac{1}{2}\log\left(\frac{x+1}{x-1}\right) & \text{if } \delta \text{ odd} \end{cases} \tag{2.8}$$

and

$$I_E(x) = \begin{cases} (-1)^{\delta/2+1}\left(\sum_{k=1}^{\delta/2-1} \frac{(-1)^k}{2k} x^{2k} + \frac{1}{2}\log(x^2+1)\right) & \text{if } \delta \text{ even} \\ (-1)^{(\delta-1)/2}\left(\sum_{k=1}^{(\delta-1)/2} \frac{(-1)^k}{2k-1} x^{2k-1} + \frac{1}{2}\tan^{-1}(x)\right) & \text{if } \delta \text{ odd}\,. \end{cases} \tag{2.9}$$

The UV cutoff M_S is introduced as the effective theory approach loses its validity beyond the scale M_S.

2.2 Details of the implementation

The virtual corrections are calculated by the one-loop generator GoSam [30]. The program combines cut-based integrand reduction techniques [31–35] with improved tensor reduction methods [36, 37]. The rational part can be calculated algebraically within GoSam in an automated way. GoSam is publicly available at `http://gosam.hepforge.org/`.

In more detail, the code generation proceeds as follows. GoSam reads an input card edited by the user and generates the diagrams and the corresponding expressions for the loop amplitudes, using `QGRAF` [38] and `FORM` [39, 40] in combination with `Spinney` [41] for the spinor algebra, and `haggies` [42] for optimisation and automated code generation. The reduction can be performed in several ways, using integrand reduction based on Samurai [34] or tensor reduction based on `Golem95C` [36, 37], or a combination of the two [35]. The basis integrals are taken from `Golem95C` or `OneLOop` [43].

For models beyond the Standard Model, model files generated by `FeynRules`[44] in the `UFO` (Universal Feynrules Output) [45] format can be imported directly by GoSam. For the process under consideration, GoSam has been extended to be able to deal with spin-2 particles, and a version of the `Golem95C` library is used which contains integrals where the tensor rank r exceeds the number N of propagators [46]. The extension of the reduction at integrand level to cases where $r = N + 1$ has been worked out in [47].

For the QCD part, we work in the Feynman gauge, and renormalisation has been done in the $\overline{MS}$ scheme. As the interaction between the Kaluza-Klein modes of a graviton and the Standard Model particles is via the energy-momentum tensor which is a conserved quantity, no further renormalisation procedure is needed.

The generated code can then be linked to Monte Carlo programs providing the real emission and infrared subtraction parts and the phase space integration, either directly or via the Binoth Les Houches Interface [48]. A flowchart of the procedure described above is shown in Fig. 1.

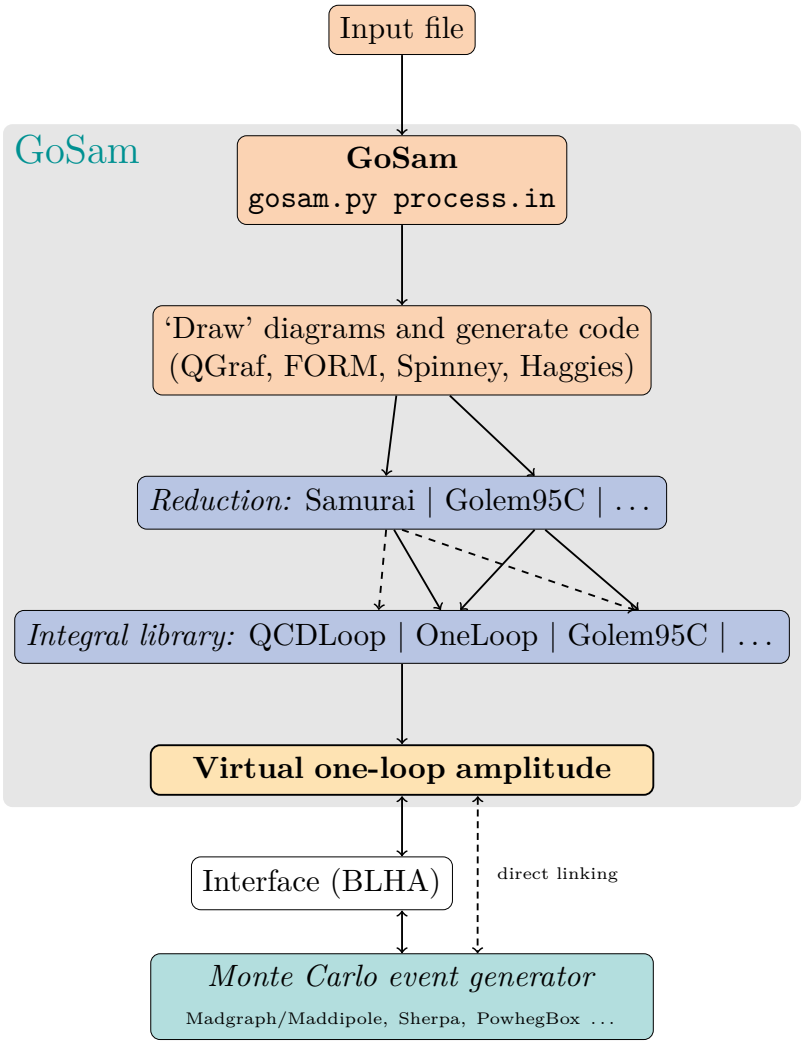


Figure 1: Workflow of the program package GoSam.

The tree level, NLO real radiation and the infrared subtraction terms have been produced with `MadDipole/MadGraph4` [49–53] and have been checked by verifying the independence of the result from the unphysical phase space cut parameter α [54]. The phase space integration of all ingredients has been performed with `MadEvent` [52, 53]. We have implemented the graviton propagator in the form of eq. (2.7) explicitly in the `Helas` routines described in [22]. In order to make sure that the conventions and the implementation of the non-standard propagator are consistent between GoSam and the Monte Carlo program providing the real radiation part, the leading order results of GoSam have been compared with the ones of `MadGraph4` [22, 51, 53] and `Sherpa` [17, 55] both at matrix element level and at cross section level.

It also has been checked that after UV renormalisation, all poles from the virtual contributions cancel with the poles from the infrared insertion operator [56] in the real radiation.

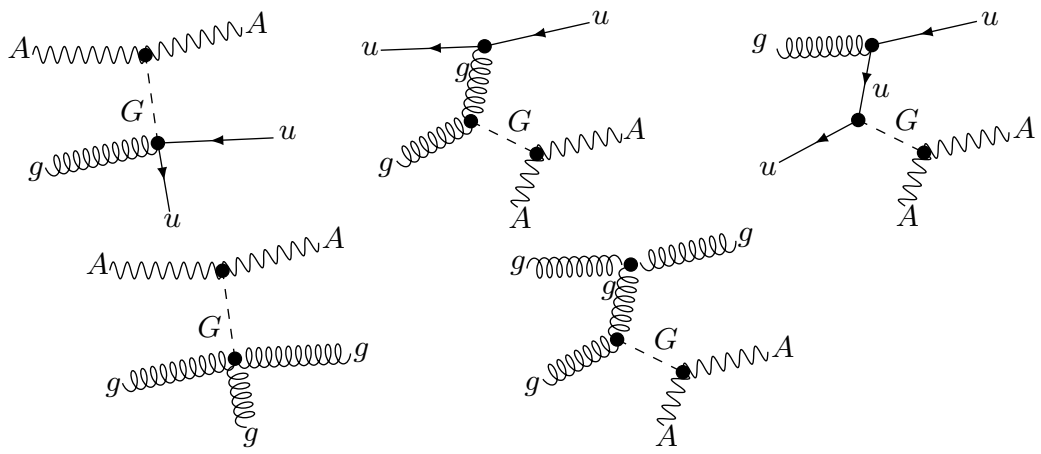


Figure 2: Tree level diagrams contributing to the process $pp \to (G \to \gamma\gamma)$+jet. Diagrams which can be obtained by crossing or summing over quark flavours are not shown.

At tree level, the following subprocesses contribute before summing over flavours (processes with $p_1 \leftrightarrow p_2$ are not shown)

$$\begin{aligned} q\bar{q} &\to (G \to \gamma\gamma) + g \\ gq &\to (G \to \gamma\gamma) + q \\ g\bar{q} &\to (G \to \gamma\gamma) + \bar{q} \\ gg &\to (G \to \gamma\gamma) + g, \end{aligned}$$

where the gg subprocess dominates at the LHC. The topologically different leading order diagrams are shown in Fig. 2.

As the gq and $g\bar{q}$ initiated subprocesses can be obtained from the $q\bar{q}$ initiated one by crossing, GoSam only generates the virtual corrections for the $u\bar{u}$ and gg initial states. The sum over flavours is performed when convoluting with the PDFs. Examples of one-loop diagrams are shown in Fig. 3.

The $u\bar{u}$ initiated subprocess contains 48 diagrams at NLO, the gg initiated one 121 diagrams. Among the latter are rank five box diagrams, which lead to complicated expressions due to the high tensor rank. The program uses the `Golem95C` library, with an extension for integrals with tensor ranks exceeding the number of propagators [46] to compute tensor integrals. Interference between signal and background processes has been neglected.

The interaction of the gravitons is described by an effective theory which loses its validity for partonic energies $\sqrt{\hat{s}} \sim M_S$. Therefore we perform the phase space integration using a cutoff $\sqrt{\hat{s}^{\max}} = M_S - \delta_{\text{cut}}$ with the default value $\delta_{\text{cut}} = 10\,\text{GeV}$. Partial wave

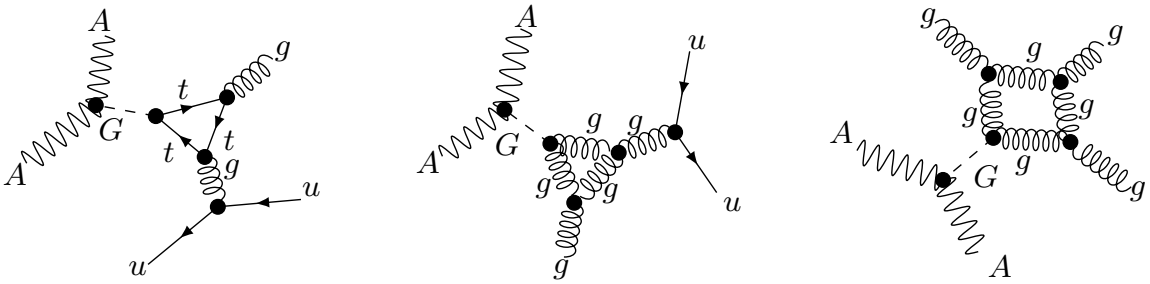


Figure 3: Selected loop level diagrams. The couplings to the spin-two particle (dashed lines) lead to tensor ranks exceeding the number of propagators in the loop integrals.

analysis in the context of longitudinal W boson scattering through the exchange of a spin-2 particle [26] has shown that the unitarity bound is not reached below the few TeV range. In our case, only couplings of the spin-2 particle to photons and QCD partons enter, therefore we do not expect the unitarity bound to set in earlier than in the case considered in Ref [26]. We refrain from the introduction of form factors to unitarize the amplitude. Due to the unknown UV completion, the choice of the parameters for the form factors remains ad hoc, except for the fact that they should "smear out" the hard phase space cutoff. We checked the cutoff dependence by variation of the cutoff, as shown in Fig. 8, and find that the cutoff dependence is rather weak, except close to the boundary of phase space $\sqrt{\hat{s}} \sim M_S$ where the effective theory description is not trustworthy anyway.

3 Phenomenological results

We now present phenomenological results for the process $pp \to (G \to \gamma\gamma)$+1 jet+X at NLO, where the two photons stem from graviton decay, for proton-proton collisions at $\sqrt{s} = 8$ GeV.

3.1 Setup, input parameters and cuts

We use the CT10 [57] parton distributions with $N_F = 5$ massless flavours and the value of α_s provided by the PDFs. For the top mass we take $m_t = 174$ GeV, the top width is set to zero. The jet clustering is done by FastJet [58, 59] using the anti-k_T algorithm [60] with a cone size of $R = 0.4$.

The ADD scale $M_S = 4$ TeV and $\delta = 4$ extra dimensions are assumed, unless stated otherwise. The renormalisation and factorisation scales are set dynamically as

$$\mu_0^2 = \mu_F^2 = \frac{1}{4}\left(m_{\gamma\gamma}^2 + p_{T,jet}^2\right) \tag{3.1}$$

with the invariant mass of the photon pair

$$m_{\gamma\gamma} = \sqrt{(p_{\gamma_1} + p_{\gamma_2})^2}\,. \tag{3.2}$$

	cross section [fb]	MC error [fb]	scale uncertainty [fb]	
LO	1.561	$\pm 6.5 \times 10^{-4}$	$^{+0.522}_{-0.363}$	$\mu=\mu_0/2$ $\mu=2\mu_0$
NLO	1.767	$\pm 7.1 \times 10^{-3}$	$^{-0.02}_{-0.11}$	$\mu=\mu_0/2$ $\mu=2\mu_0$

Table 1: LO and NLO total cross sections and theoretical uncertainties.

For the photons, the following cuts are applied:

$$p_{T,\gamma} \geq 25 \text{ GeV} \ , \ |\eta_\gamma| \leq 2.5 \ , \ 0.4 \leq \Delta R_{\gamma\gamma}. \tag{3.3}$$

Additionally, the invariant mass of the photon pair is restricted to

$$140 \text{ GeV} \leq m_{\gamma\gamma} < 3.99 \text{ TeV}. \tag{3.4}$$

The lower bound serves to suppress the Standard Model background. The jets are restricted by the following cuts:

$$p_{T,\text{leading jet}} \geq 30 \text{ GeV} \ , \ |\eta_{\text{jet}}| \leq 4 \ , \ 0.4 \leq \Delta R_{\text{jet},\gamma} \ . \tag{3.5}$$

The SM background can be suppressed considerably by choosing very large values for $p_{T,\gamma}^{\min}$ and $m_{\gamma\gamma}^{\min}$. In our calculation we choose rather moderate cuts, which are motivated by the ones used in [12].

3.2 Results

The results for the total cross sections are shown in Table 1. The scale uncertainty improves significantly between LO and NLO, as can be seen from Table 1 and Fig. 4.

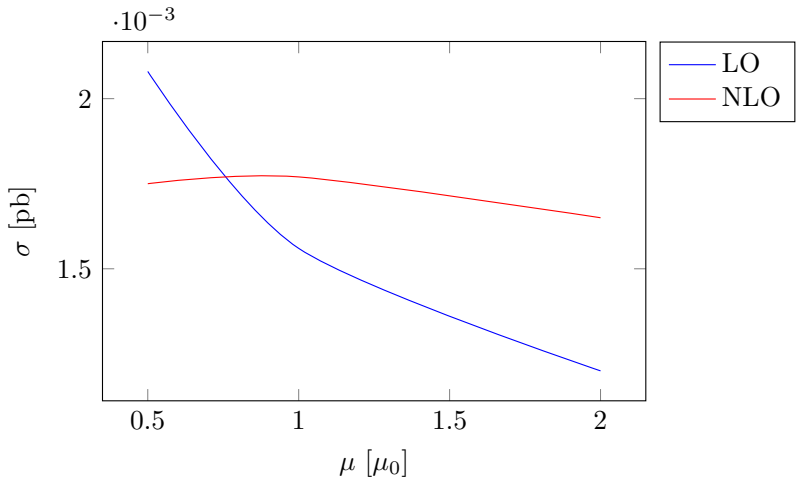


Figure 4: Behaviour of the cross section under scale variations, varying by a factor two around the central scale defined in eq. (3.1).

One of the most important observables in searches for extra dimensions based on graviton decay into two photons is the diphoton invariant mass spectrum, as we expect large enhancements in the tail of the $m_{\gamma\gamma}$ distribution.

Fig. 5 shows the invariant mass distribution of the photon pair at LO and NLO. We observe that the K-factor is far from being constant for this distribution, increasing towards large values of $m_{\gamma\gamma}$. In order to verify that this behaviour of the K-factor is not an artifact of the dynamical scale choice, we have also made the calculation with a fixed scale of 2 TeV and found a similar behaviour of the K-factor. Therefore the procedure to take NLO corrections into account by rescaling the leading order distribution by a constant K-factor, as has been done in all experimental analyses so far, can only give a rough estimate of the NLO corrections.

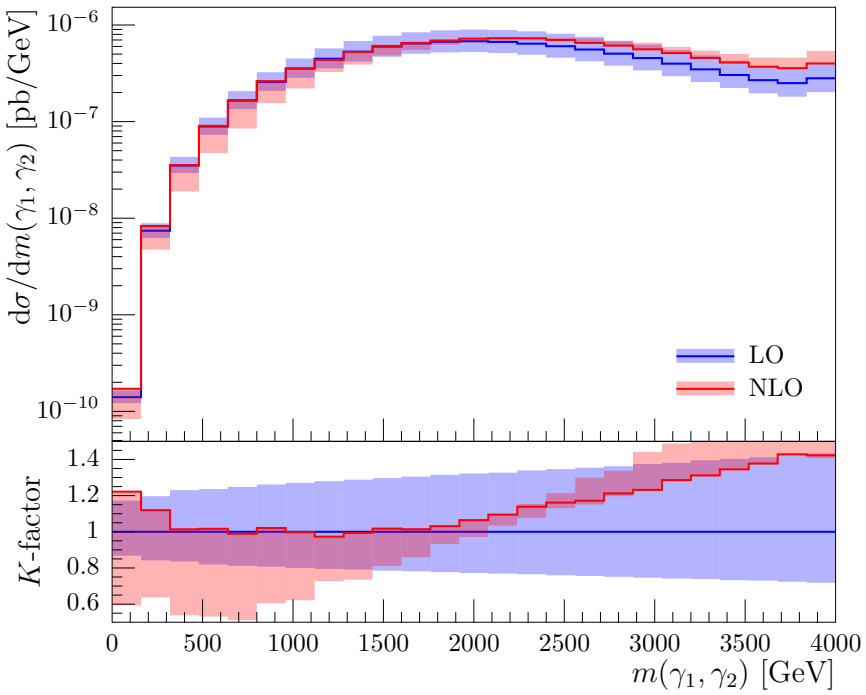


Figure 5: NLO QCD corrections to the invariant mass distribution of the photon pair stemming from graviton decay. The bands show the scale variations by a factor of two around the central scale.

In Fig. 6 the invariant mass distribution of the photon pair is compared to the LO Standard Model background. The latter has been rescaled by a factor of 10^{-3} in order to be able to compare the shapes. It is obvious that the shape of the background for the $m_{\gamma\gamma}$ distribution is very different, and an enhancement over the background should be visible in the large $m_{\gamma\gamma}$ region within ADD models.

Large variations of the differential K-factor can also be observed in the transverse momentum distributions of the photons and of the jet. The K-factor of the leading-p_T photon, γ_1, is also increasing towards large p_T values, as shown in Fig. 7a, while the differential K-factor for the transverse momentum distribution of the jet is decreasing as the p_T of the jet is increasing, see Fig. 7b. The softening of the jet p_T spectrum at NLO can be understood from the fact that at high p_T, a single jet (parton) is more likely to radiate another parton – which only is taken into account at NLO – and this makes the

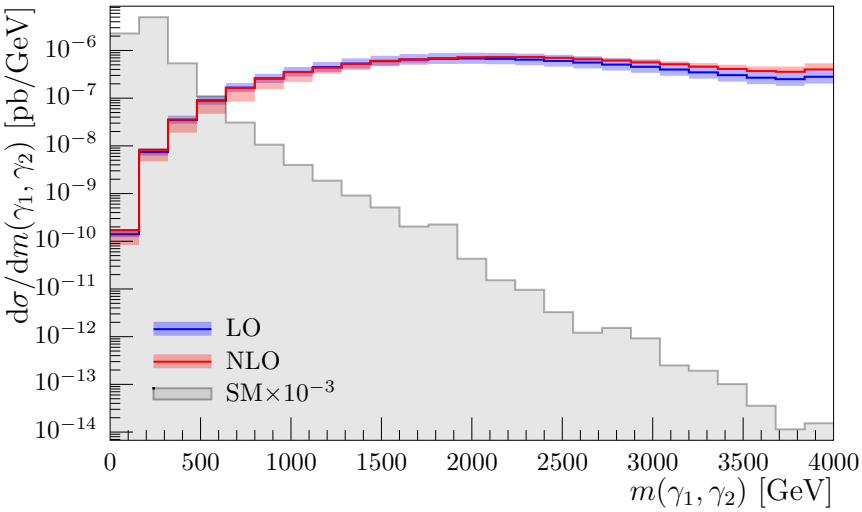
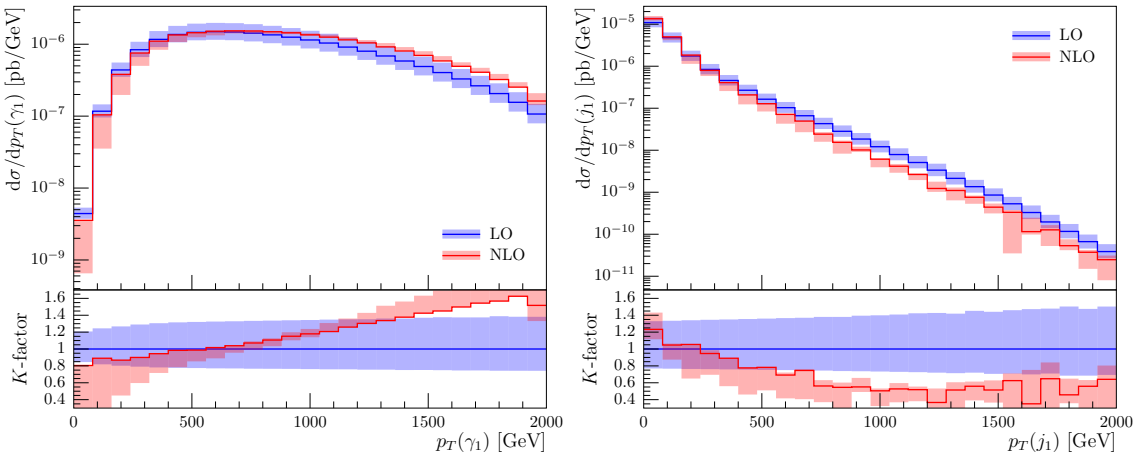


Figure 6: Invariant mass of the photon pair at LO and NLO. The bands show the scale variations by a factor of two around the central scale. The SM background, rescaled by a factor of 10^{-3}, is also shown.

original jet softer.



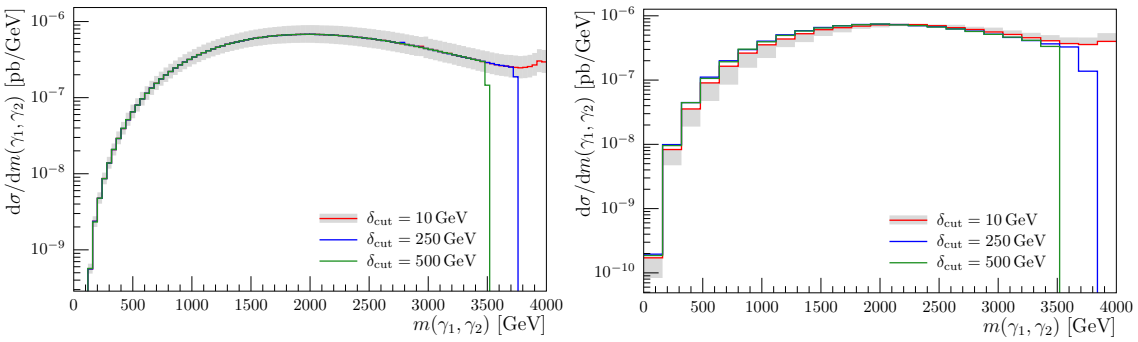
(a) p_T distribution of the leading photon

(b) p_T distribution of the jet

Figure 7: NLO QCD corrections to the transverse momentum distribution of (a) the leading-p_T photon and (b) the jet. The bands show the scale variations by a factor of two around the central scale.

As we are calculating the QCD corrections to a process involving only graviton bridges, while graviton loops are suppressed, the unknown UV completion of the theory should not destroy the reliability of the QCD corrections below the scale M_S. In order to test the dependence on the cutoff scale in the phase space integration, we varied $\sqrt{\hat{s}^{\max}} = M_S - \delta_{\text{cut}}$ using $\delta_{\text{cut}} = 10, 250, 500\,\text{GeV}$. At LO, except for the region very close to the cutoff, the dependence of the shape on δ_{cut} is weaker than the residual scale dependence, as can be

seen from Fig. 8a. At NLO, the scale uncertainty is considerably reduced, therefore the relative size of the two types of uncertainties does not show this clear hierarchy anymore. Nonetheless one can see from Fig. 8b that the δ_{cut}-dependence is very weak for almost the whole range of the distribution, being limited to a small region around the cutoff scale. Certainly, the size of the total cross section will depend on the cutoff, but normalized distributions will show their characteristic shape, independent of the precise value of the cutoff (as long as it is in the vicinity of M_S). This behaviour confirms that the NLO QCD corrections are not affected to an unacceptable extent by the unknown UV completion of the model.



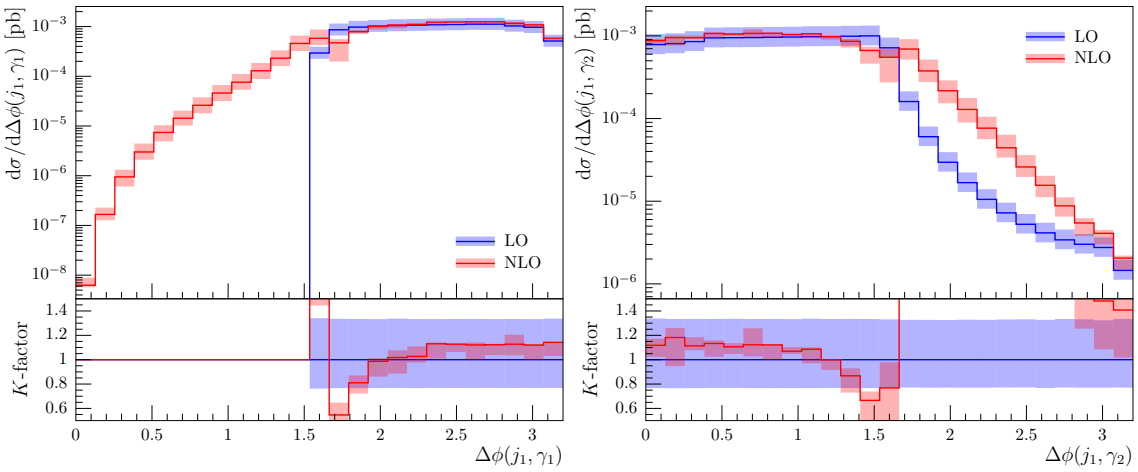
(a) LO (b) NLO

Figure 8: Dependence of the diphoton invariant mass distribution on the value of the cutoff $\sqrt{\hat{s}^{\max}} = M_S - \delta_{\text{cut}}$ where the effective theory is expected to loose its range of validity.

Angular distributions are particularly interesting as they can serve to pin down the spin-two nature of the object decaying into a photon pair. The presence of the jet gives us an extra handle to probe the kinematics. The relative azimuthal angle distributions between the jet and the leading respectively subleading photon are particularly interesting. Fig. 9 illustrates that the NLO corrections significantly alter the shape because the extra parton present in the real radiation contribution opens up a region which is kinematically inaccessible at LO. Even though this feature certainly is also present in the SM background, Fig. 9 clearly displays the importance of NLO corrections.

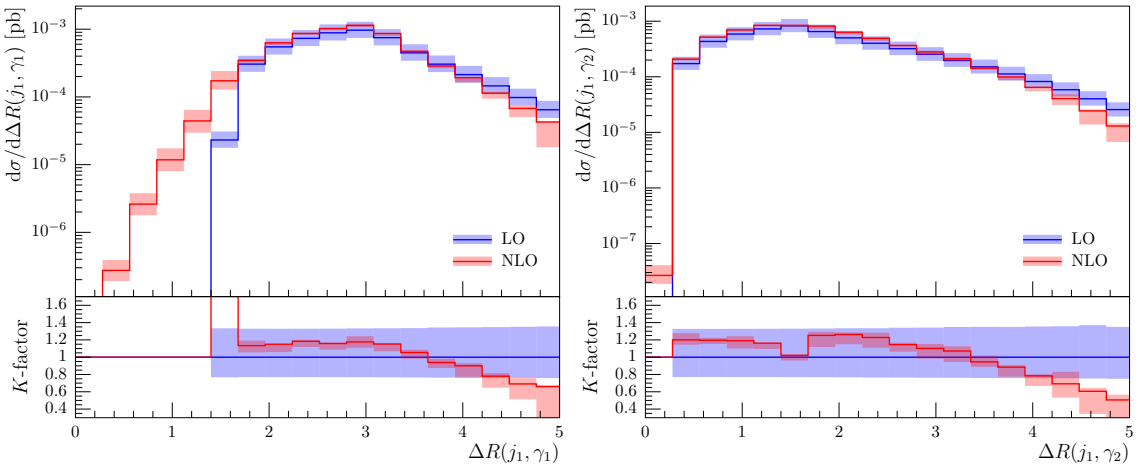
In Fig. 10 the distributions for the distance in rapidity and azimuthal angle space $\Delta R(j,\gamma) = \sqrt{(\eta^j - \eta^\gamma)^2 + (\varphi^j - \varphi^\gamma)^2}$ between the jet and the leading and subleading-p_T photon are shown. Fig. 11 displays the rapidity distributions of the leading photon respectively the jet. Again, the non-uniform K-factors are clearly visible.

Finally, we also investigate the case of five or six extra dimensions rather than four. The higher the number of extra dimensions, the weaker the exclusion limits, as the total cross section decreases with increasing dimensions. As can be seen from Figs. 12 and 13, the qualitative behaviour is rather similar for different numbers of extra dimensions, even though the propagator has a different analytic form for odd numbers of extra dimensions.



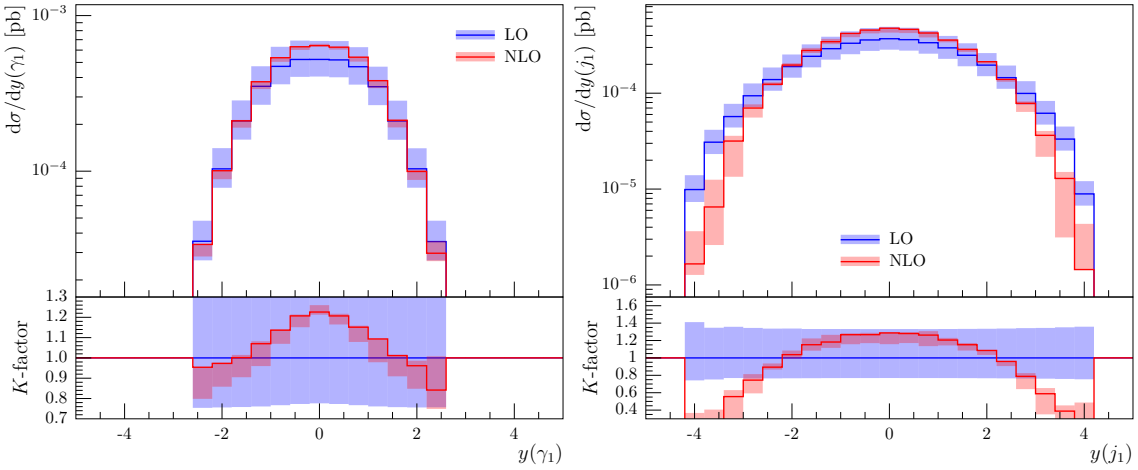
(a) (b)

Figure 9: Distribution of the relative azimuthal angle $\Delta\varphi$ between the jet and (a) the leading-p_T photon, (b) the subleading-p_T photon.



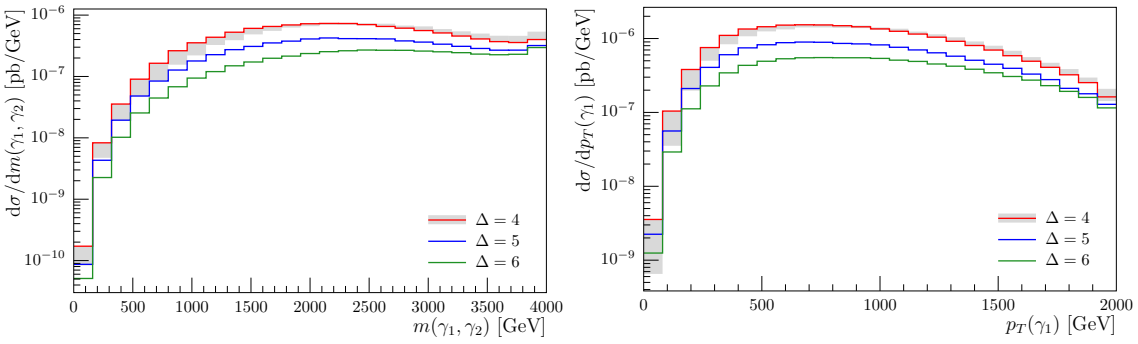
(a) (b)

Figure 10: Distribution of the distance ΔR between the jet and (a) the leading-p_T photon, (b) the subleading-p_T photon.



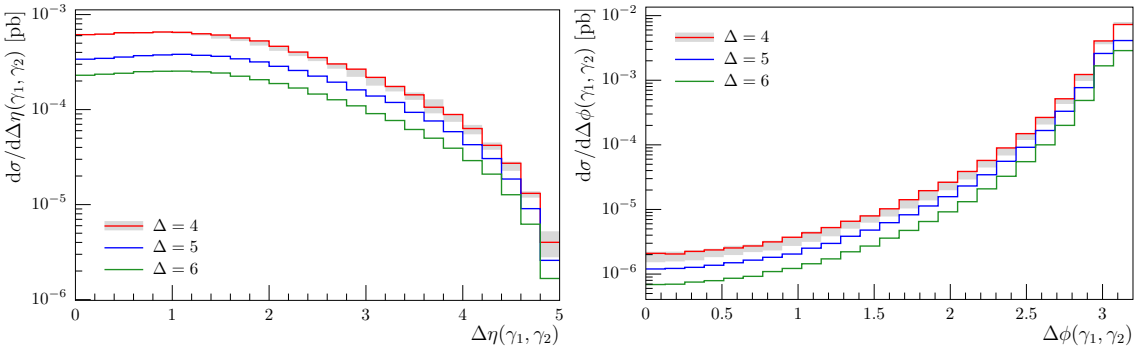
(a) (b)

Figure 11: Rapidity distributions for (a) the leading-p_T photon, (b) the jet.



(a) (b)

Figure 12: (a) Diphoton invariant mass and (b) transverse momentum distribution for different numbers of extra dimensions at NLO. The scale uncertainty band is only included for $\Delta = 4$.



(a) (b)

Figure 13: (a) Diphoton rapidity difference and (b) relative azimuthal angle distributions for different numbers of extra dimensions at NLO.

4 Conclusions

We have calculated the NLO QCD corrections to the process $pp \to (G \to \gamma\gamma)+\text{jet}+\text{X}$ within the ADD [15] model of large extra dimensions.

The one-loop part of the calculation has been provided by the automated program package GoSam, which is publicly available at `http://gosam.hepforge.org/`. GoSam can import any Beyond the Standard Model file in `UFO` (Universal Feynrules Output) format and can deal with effective vertices and particles up to spin two. For the real radiation parts we used the `MadDipole/MadGraph4` framework. As the effective field theory approximation breaks down for energies exceeding the fundamental scale of quantum gravity (which is supposed to be in the TeV range for ADD models), the phase space integrations have been restricted to center of mass energies below the scale $M_S \sim 4\,\text{TeV}$. We have studied the UV cutoff dependence in detail and demonstrated that the latter does not affect the distributions significantly, except for a small region close to the cutoff value.

The corrections significantly reduce the scale uncertainty and lead to K-factors for the total cross section of the order of 1.1 to 1.4. It is important to note that the differential K-factors are far from being constant. For the diphoton invariant mass distribution as well as for the photon transverse momentum distributions the K-factors increase up to about 1.5 towards the tail of the distributions, while for the jet p_T distribution, the behaviour is the opposite.

We have studied the cases $\delta = 4, 5, 6$ extra dimensions and find similar qualitative behaviour, while the cross sections are decreasing as the number of extra dimensions grows. We also investigate angular distributions where the NLO corrections significantly change the shape, as kinematic regions open up which are not accessible at leading order.

This calculation illustrates the power and flexibility of GoSam to do one-loop calculations for multi-particle final states stemming from interactions beyond the Standard Model. Further applications in this direction will hopefully be confronted with data hinting to BSM physics in the not too distant future.

Acknowledgments

We would like to thank all the members of the GoSam collaboration for contributions to code development and constructive comments. We also thank Dorival Goncalves-Netto and Dieter Zeppenfeld for interesting discussions. We further acknowledge computing support of the Rechenzentrum Garching.

References

[1] **ATLAS** Collaboration, G. Aad et al., *Observation of a new particle in the search for the Standard Model Higgs boson with the ATLAS detector at the LHC*, *Phys.Lett.* **B716** (2012) 1–29, [arXiv:1207.7214].

[2] **CMS** Collaboration, S. Chatrchyan et al., *Observation of a new boson at a mass of 125 GeV with the CMS experiment at the LHC*, *Phys.Lett.* **B716** (2012) 30–61, [arXiv:1207.7235].

[3] **ATLAS** Collaboration, G. Aad et al., *Evidence for the spin-0 nature of the Higgs boson using ATLAS data*, arXiv:1307.1432.

[4] *Study of the spin of the new boson with up to 25 fb^{-1} of ATLAS data*, Tech. Rep. ATLAS-CONF-2013-040, CERN, Geneva, Apr, 2013.

[5] *Study of the spin properties of the Higgs-like particle in the $H \to WW$ channel with 21 fb^{-1} of $\sqrt{s}$=8 TeV data collected with the ATLAS detector*, Tech. Rep. ATLAS-CONF-2013-31, CERN, Geneva, Mar, 2013.

[6] *Study of the spin of the Higgs-like boson in the two photon decay channel using 20.7 fb^{-1} of pp collisions collected at $\sqrt{s}$ = 8 TeV with the ATLAS detector*, Tech. Rep. ATLAS-CONF-2013-29, CERN, Geneva, Mar, 2013.

[7] *Combination of standard model Higgs boson searches and measurements of the properties of the new boson with a mass near 125 GeV*, Tech. Rep. CMS-PAS-HIG-13-005, CERN, Geneva, 2013.

[8] *Evidence for a particle decaying to W+W- in the fully leptonic final state in a standard model Higgs boson search in pp collisions at the LHC*, Tech. Rep. CMS-PAS-HIG-13-003, CERN, Geneva, Mar, 2013.

[9] J. Ellis, R. Fok, D. S. Hwang, V. Sanz, and T. You, *Distinguishing 'Higgs' Spin Hypotheses using gamma gamma and WW* Decays*, arXiv:1210.5229.

[10] J. Ellis, V. Sanz, and T. You, *Prima Facie Evidence against Spin-Two Higgs Impostors*, arXiv:1211.3068.

[11] **ATLAS** Collaboration, G. Aad et al., *Search for Extra Dimensions using diphoton events in 7 TeV proton-proton collisions with the ATLAS detector*, *Phys.Lett.* **B710** (2012) 538–556, [arXiv:1112.2194].

[12] **ATLAS** Collaboration, G. Aad et al., *Search for Extra Dimensions in diphoton events using proton-proton collisions recorded at $\sqrt{s} = 7$ TeV with the ATLAS detector at the LHC*, *New J.Phys.* **15** (2013) 043007, [arXiv:1210.8389].

[13] **CMS** Collaboration, S. Chatrchyan et al., *Search for Large Extra Dimensions in the Diphoton Final State at the Large Hadron Collider*, *JHEP* **1105** (2011) 085, [arXiv:1103.4279].

[14] **CMS** Collaboration, S. Chatrchyan et al., *Search for signatures of extra dimensions in the diphoton mass spectrum at the Large Hadron Collider*, *Phys.Rev.Lett.* **108** (2012) 111801, [arXiv:1112.0688].

[15] N. Arkani-Hamed, S. Dimopoulos, and G. Dvali, *The Hierarchy problem and new dimensions at a millimeter*, *Phys.Lett.* **B429** (1998) 263–272, [hep-ph/9803315].

[16] T. Han, J. D. Lykken, and R.-J. Zhang, *On Kaluza-Klein states from large extra dimensions*, *Phys.Rev.* **D59** (1999) 105006, [hep-ph/9811350].

[17] T. Gleisberg, F. Krauss, K. T. Matchev, A. Schalicke, S. Schumann, et al., *Helicity formalism for spin-2 particles*, *JHEP* **0309** (2003) 001, [hep-ph/0306182].

[18] M. Kumar, P. Mathews, V. Ravindran, and A. Tripathi, *Diphoton signals in theories with large extra dimensions to NLO QCD at hadron colliders*, *Phys.Lett.* **B672** (2009) 45–50, [arXiv:0811.1670].

[19] M. Kumar, P. Mathews, V. Ravindran, and A. Tripathi, *Direct photon pair production at the LHC to order α_s in TeV scale gravity models*, *Nucl.Phys.* **B818** (2009) 28–51, [arXiv:0902.4894].

[20] R. Frederix, M. K. Mandal, P. Mathews, V. Ravindran, S. Seth, et al., *Diphoton production in the ADD model to NLO+parton shower accuracy at the LHC*, *JHEP* **1212** (2012) 102, [arXiv:1209.6527].

[21] P. Artoisenet, P. de Aquino, F. Demartin, R. Frederix, S. Frixione, et al., *A framework for Higgs characterisation*, arXiv:1306.6464.

[22] P. de Aquino, K. Hagiwara, Q. Li, and F. Maltoni, *Simulating graviton production at hadron colliders*, *JHEP* **1106** (2011) 132, [arXiv:1101.5499].

[23] R. Frederix, M. Mandal, P. Mathews, V. Ravindran, and S. Seth, *Drell-Yan, ZZ, W+W-production in SM & ADD model to NLO+PS accuracy at the LHC*, arXiv:1307.7013.

[24] Karg, Stefan and Krämer, Michael and Li, Qiang and Zeppenfeld, Dieter, *NLO QCD corrections to graviton production at hadron colliders*, *Phys.Rev.* **D81** (2010) 094036, [arXiv:0911.5095].

[25] J. Frank, M. Rauch, and D. Zeppenfeld, *Spin-2 Resonances in Vector-Boson-Fusion Processes at NLO QCD*, arXiv:1211.3658.

[26] J. Frank, *Spin-2 Resonances in Vector Boson Fusion Processes at the LHC*, *Diploma thesis, Karlsruhe Institute of Technology* (2011).

[27] V. Del Duca, F. Maltoni, Z. Nagy, and Z. Trocsanyi, *QCD radiative corrections to prompt diphoton production in association with a jet at hadron colliders*, *JHEP* **0304** (2003) 059, [hep-ph/0303012].

[28] T. Gehrmann, N. Greiner, and G. Heinrich, *Photon isolation effects at NLO in $\gamma\gamma$ + jet final states in hadronic collisions*, *JHEP* **1306** (2013) 058, [arXiv:1303.0824].

[29] G. F. Giudice, R. Rattazzi, and J. D. Wells, *Quantum gravity and extra dimensions at high-energy colliders*, *Nucl.Phys.* **B544** (1999) 3–38, [hep-ph/9811291].

[30] G. Cullen, N. Greiner, G. Heinrich, G. Luisoni, P. Mastrolia, et al., *Automated One-Loop Calculations with GoSam*, *Eur.Phys.J.* **C72** (2012) 1889, [arXiv:1111.2034].

[31] G. Ossola, C. G. Papadopoulos, and R. Pittau, *Reducing full one-loop amplitudes to scalar integrals at the integrand level*, *Nucl.Phys.* **B763** (2007) 147–169, [hep-ph/0609007].

[32] R. Ellis, W. Giele, and Z. Kunszt, *A Numerical Unitarity Formalism for Evaluating One-Loop Amplitudes*, *JHEP* **0803** (2008) 003, [arXiv:0708.2398].

[33] P. Mastrolia, G. Ossola, C. Papadopoulos, and R. Pittau, *Optimizing the Reduction of One-Loop Amplitudes*, *JHEP* **0806** (2008) 030, [arXiv:0803.3964].

[34] P. Mastrolia, G. Ossola, T. Reiter, and F. Tramontano, *Scattering AMplitudes from Unitarity-based Reduction Algorithm at the Integrand-level*, *JHEP* **1008** (2010) 080, [arXiv:1006.0710].

[35] G. Heinrich, G. Ossola, T. Reiter, and F. Tramontano, *Tensorial Reconstruction at the Integrand Level*, *JHEP* **1010** (2010) 105, [arXiv:1008.2441].

[36] T. Binoth, J.-P. Guillet, G. Heinrich, E. Pilon, and T. Reiter, *Golem95: A Numerical program to calculate one-loop tensor integrals with up to six external legs*, *Comput.Phys.Commun.* **180** (2009) 2317–2330, [arXiv:0810.0992].

[37] G. Cullen, J. Guillet, G. Heinrich, T. Kleinschmidt, E. Pilon, et al., *Golem95C: A library for one-loop integrals with complex masses*, *Comput.Phys.Commun.* **182** (2011) 2276–2284, [arXiv:1101.5595].

[38] P. Nogueira, *Automatic Feynman graph generation*, *J.Comput.Phys.* **105** (1993) 279–289.

[39] J. Vermaseren, *New features of FORM*, math-ph/0010025.

[40] J. Kuipers, T. Ueda, J. Vermaseren, and J. Vollinga, *FORM version 4.0*, arXiv:1203.6543.

[41] G. Cullen, M. Koch-Janusz, and T. Reiter, *Spinney: A Form Library for Helicity Spinors*, *Comput.Phys.Commun.* **182** (2011) 2368–2387, [arXiv:1008.0803].

[42] T. Reiter, *Optimising Code Generation with haggies*, *Comput.Phys.Commun.* **181** (2010) 1301–1331, [arXiv:0907.3714].

[43] A. van Hameren, *OneLOop: For the evaluation of one-loop scalar functions*, *Comput.Phys.Commun.* **182** (2011) 2427–2438, [arXiv:1007.4716].

[44] N. D. Christensen and C. Duhr, *FeynRules - Feynman rules made easy*, *Comput.Phys.Commun.* **180** (2009) 1614–1641, [arXiv:0806.4194].

[45] C. Degrande, C. Duhr, B. Fuks, D. Grellscheid, O. Mattelaer, et al., *UFO - The Universal FeynRules Output*, *Comput.Phys.Commun.* **183** (2012) 1201–1214, [arXiv:1108.2040].

[46] J.-P. Guillet, G. Heinrich, and von Soden-Fraunhofen, J.F., *Tools for spin two particles: extension of the golem95C integral library*, *in preparation* (2013).

[47] P. Mastrolia, E. Mirabella, and T. Peraro, *Integrand reduction of one-loop scattering amplitudes through Laurent series expansion*, *JHEP* **1206** (2012) 095, [arXiv:1203.0291].

[48] T. Binoth, F. Boudjema, G. Dissertori, A. Lazopoulos, A. Denner, et al., *A Proposal for a standard interface between Monte Carlo tools and one-loop programs*, *Comput.Phys.Commun.* **181** (2010) 1612–1622, [arXiv:1001.1307].

[49] R. Frederix, T. Gehrmann, and N. Greiner, *Automation of the Dipole Subtraction Method in MadGraph/MadEvent*, *JHEP* **0809** (2008) 122, [arXiv:0808.2128].

[50] R. Frederix, T. Gehrmann, and N. Greiner, *Integrated dipoles with MadDipole in the MadGraph framework*, *JHEP* **1006** (2010) 086, [arXiv:1004.2905].

[51] T. Stelzer and W. Long, *Automatic generation of tree level helicity amplitudes*, *Comput.Phys.Commun.* **81** (1994) 357–371, [hep-ph/9401258].

[52] F. Maltoni and T. Stelzer, *MadEvent: Automatic event generation with MadGraph*, *JHEP* **0302** (2003) 027, [hep-ph/0208156].

[53] J. Alwall, P. Demin, S. de Visscher, R. Frederix, M. Herquet, et al., *MadGraph/MadEvent v4: The New Web Generation*, *JHEP* **0709** (2007) 028, [arXiv:0706.2334].

[54] Z. Nagy and Z. Trocsanyi, *Next-to-leading order calculation of four jet observables in electron positron annihilation*, *Phys.Rev.* **D59** (1999) 014020, [hep-ph/9806317].

[55] T. Gleisberg, S. Hoeche, F. Krauss, M. Schonherr, S. Schumann, et al., *Event generation with SHERPA 1.1*, *JHEP* **0902** (2009) 007, [arXiv:0811.4622].

[56] S. Catani and M. Seymour, *A General algorithm for calculating jet cross-sections in NLO QCD*, *Nucl.Phys.* **B485** (1997) 291–419, [hep-ph/9605323].

[57] H.-L. Lai, M. Guzzi, J. Huston, Z. Li, P. M. Nadolsky, et al., *New parton distributions for collider physics*, *Phys.Rev.* **D82** (2010) 074024, [arXiv:1007.2241].

[58] M. Cacciari and G. P. Salam, *Dispelling the N^3 myth for the k_t jet-finder*, *Phys.Lett.* **B641** (2006) 57–61, [hep-ph/0512210].

[59] M. Cacciari, G. P. Salam, and G. Soyez, *FastJet User Manual*, *Eur.Phys.J.* **C72** (2012) 1896, [arXiv:1111.6097].

[60] M. Cacciari, G. P. Salam, and G. Soyez, *The Anti-k(t) jet clustering algorithm*, *JHEP* **0804** (2008) 063, [arXiv:0802.1189].